



Identifying soil water movement and water sources of subsurface flow at a hillslope using stable isotope technique

R.X. Zhou^a, J. Wang^{a,*}, C.J. Tang^b, Y.P. Zhang^a, X.A. Chen^b, X. Li^a, Y.Y. Shi^a, L. Wang^a, H.B. Xiao^a, Z.H. Shi^a

^a State Environmental Protection Key Laboratory of Soil Health and Green Remediation, Huazhong Agricultural University, Wuhan 430070, China

^b Jiangxi Provincial Key Laboratory of Soil Erosion and Prevention, Jiangxi Academy of Water Science and Engineering, Nanchang, Jiangxi 330029, China



ARTICLE INFO

Keywords:
Subsurface flow
Stable isotope
Water sources
Soil water movement
MixSIAR
Farming practice

ABSTRACT

Knowledge concerning soil water movement and water sources of subsurface flow is crucial for understanding runoff generation mechanisms and nutrient-pollution migration. Although the spatiotemporal characteristics of soil water have been confirmed, water sources of subsurface flow during rainfall remain poorly understood at the hillslope scale. We measured the $\delta^{18}\text{O}$ and $\delta^2\text{H}$ in soil water before and after storm events to explore the mixing process of new water (rainwater) and old water (pre-event soil water) at the hillslopes with different farming practices (bare land, no-tillage and straw mulching). Water source partitioning of subsurface flow during three storms (April 11, April 24, June 10) were quantified using the MixSIAR model. The results showed that both preferential flow and piston flow existed in the process of soil water movement which were detected by the variation in the isotopic values of soil water after storms. The proportional contributions of new water to subsurface flow from 0–30 cm in no-tillage plot was the highest (46.60%) among experimental plots. The fraction of new water to subsurface flow for no-tillage, bare land, and straw mulching plot was 27.36%, 22.39%, and 16.28%, respectively, indicating that farming practices affected water source partitioning of subsurface flow. The average proportion of old water to subsurface flow of 0–30 cm, 30–60 cm and 60–90 cm during three storm events were 71.77%, 76.72%, and 87.48%, respectively, suggesting that subsurface flow was mainly derived from old water with soil depths specific responses. In addition, the proportional contributions of new water to subsurface flow varied dynamically with the progress of rainfall, implying that the mixing between new and old water affected water sources of subsurface flow. These findings have crucial implications for understanding the generation mechanisms of subsurface flow and the sustainable management of agro-environmental systems.

1. Introduction

Soil water plays a crucial role in the interaction of the atmosphere—plant—soil systems (Gazis and Feng, 2004; Sprenger et al., 2016a). The migration and transformation behavior of nutrients (e.g., carbon and nitrogen) and pollutants (e.g., microplastics and dissolved heavy metals) are affected by soil water as a medium (Pei et al., 2021). Additionally, as a significant driving force for many hydrological and ecological processes, soil water controls infiltration, pore space percolation, soil evaporation, and storage capacity, affecting the distribution of soil water and runoff generation across temporal and spatial scales (Singh et al., 2021). Identifying the process of soil water movement in the unsaturated zone provides critical insights into understanding and modeling runoff generation processes, and guiding water resource

allocation, drought and flood management (Zhang et al., 2021).

The rainwater entering the unsaturated zone is partitioned into a vapor flux that either returns to the atmosphere through evaporation and transpiration or replenishes soil water (Carpena et al., 2018). In the unsaturated zone of the hillslope, soil water is recharged principally through two mechanisms of piston flow and preferential flow. Piston flow usually occurs in soils with low porosity and relatively uniform properties (Song et al., 2009). Rainwater (new water) enters the soil to displace pre-event water (old water), pushing it deep into the soil profile until it eventually drains into rivers or recharges groundwater (Huang et al., 2020). However, cracks and macropores may act as channels for rapid water movement in heterogeneous soil, leading to preferential flow (Nimmo, 2021). Consequently, these two recharge mechanisms alter the spatial distribution of soil water and flow paths, which in turn

* Corresponding author.

E-mail address: dianwang1990@163.com (J. Wang).

affects the generation of subsurface flow. Unraveling the dominant mechanism of soil water movement is crucial to identify the water sources of subsurface flow.

Subsurface flow is a significant part of the runoff pathway and provides crucial recharge for groundwater, rivers and lakes. As the soil permeability decreases gradually with increasing depth, a relatively impervious layer forms in the soil. The infiltrated rainwater mixes with pre-existing soil water and experiences horizontal lateral flow and vertical infiltration along the soil layer interface, forming subsurface flow (Ma et al., 2022). Adequate water sources and relatively impermeable layers are necessary conditions for the generation of subsurface flow, which is affected by soil properties, rainfall characteristics and vegetation cover (Wang et al., 2020; Xiao et al., 2020a). Subsurface flow or lateral interflow affects agricultural ecological environment and production in different ways (Fei et al., 2019; Skaalsveen et al., 2019). On the one hand, nutrients that leach through subsurface flows, including nitrate, particulate phosphorus and dissolved carbon, contribute to the nutrient conditions of farmland and may simultaneously cause water resource pollution (Bai et al., 2018; Nazari et al., 2022). On the other hand, the development of subsurface flow accelerates the runoff transit time and sediment loss across multiple temporal and spatial scales (Sun et al., 2015; Skaalsveen et al., 2019). These ways have important on- and off-site impacts on agro-environmental conditions and agricultural production (Sun et al., 2015). Thus, unravelling water source partitioning of subsurface flow has profound implications for understanding hydrology-soil interactions and water sources management in agro-ecosystems. Most previous studies have focused on the generation, solute transfer, and environmental impacts of subsurface flow (Bah et al., 2020; Xiao et al., 2020a; Zoccatelli et al., 2019). However, the mixing process of new and old water and the water sources for subsurface flow during storm remain unclear.

Identifying the mixing process of new and old water in the unsaturated zone is often challenging. First, the release and storage of soil water are strongly influenced by vegetation cover, soil texture and antecedent soil moisture, and their hydrological response to spatial-temporal variations in meteorological inputs is complex (Stumpf and Hendry, 2012; Zheng et al., 2019). Second, the traditional methods to investigate the mixing process of new and old water have certain limitations that make it difficult to reveal the complexity of subsurface hydrological processes. For example, soil moisture monitoring needs to bury probes in the soil (Zhuo et al., 2020), which destroys the natural structure of the soil. The establishment of hydraulic parameter models also requires a large amount of data as a basis (Thiros et al., 2021). Additionally, some emerging technologies, such as ground penetrating radar and computed tomography scanning, do not damage natural soil structures but require sophisticated sampling equipment and high resource costs, limiting their application (Haruzi et al., 2022; Di Prima et al., 2020). The stable isotope technique offers an effective tool to solve complex hydrological problems in unsaturated zones (McDonnell et al., 1990; Beyer et al., 2020; Sprenger et al., 2016b). Hydrogen and oxygen stable isotopes in water behave conservatively and do not react with substances in the soil (Tippie et al., 2017). In addition, the sampling and measurement of $\delta^2\text{H}$ and $\delta^{18}\text{O}$ are convenient. Therefore, stable hydrogen and oxygen isotopes can be applied to reveal the mixing process of new and old water and identify the water sources of subsurface flow and their contributions to subsurface flow (Jasechko et al., 2016; Xiao et al., 2020a).

The red soil hilly region of southern China covers an area of 2.18 million km², and approximately 40% of the country's population lives in the red soil region (Wang et al., 2019a). This region is an important agricultural production base in China with abundant water and heat resources (Chen et al., 2020; Tao et al., 2021). Due to long-term cultivation of slope cropland in red soil hilly regions, the shallow soil has a loose structure and abundant pores, but deep soil is dense and has poor permeability, forming a relatively impermeable layer, which easily generates subsurface flow (Yang et al., 2020). In this study, we

investigated the mixing process of new and old water, and water sources of subsurface flow via high-frequency hydrological monitoring using stable isotope technique on a typical red soil hillslope. The objectives of this study were to (i) decipher the temporal and spatial variations in soil moisture and its isotope characteristics; (ii) probe the mixing process of new water and old water during storms; and (iii) determine the water sources of subsurface flow during storms.

2. Materials and methods

2.1. Study area

The study was conducted in the Yangou catchment ($29^{\circ}16'3''$ – $29^{\circ}17'49''$ N, $115^{\circ}42'38''$ – $115^{\circ}43'06''$ E), which is located in the Poyang Lake system in northern Jiangxi Province, China (Fig. 1). The landform of the catchment is dominated by hills, with an area of 1.23 km². The elevation ranges from 30 to 100 m, and the slope ranges from 5° to 25°. As a typical subtropical monsoon climate zone, this catchment has abundant rainfall with an uneven distribution throughout the year. The mean annual rainfall and temperature are 1469 mm and 16.7 °C, respectively. The local soil in this region is mainly red clay soil and an Ultisols according to the USDA soil taxonomy (Soil Survey Staff, 1999).

2.2. Experimental design and sampling

The study was conducted on three sloping experimental plots with different farming practices, including no-tillage, straw mulching and bare land. Each plot had a similar area, orientation and slope and represented typical sloping farmland in the catchment. The crop in the sloping experimental plot was peanuts, and there was no irrigation during the study period. The soil physicochemical properties within the plots are shown in Table 1. The soil particle size distribution of the sloping experimental plots was mainly silt and clay.

The tipping bucket rain gauge with an error of 0.1 mm (Onset Computer Corporation, MA, USA) was placed near the experimental plots to monitor storm events. The start and end times of storm events and rainfall intensity were recorded. Soil water content (SWC) and soil temperature were measured by time domain reflectometry sensors (100, Campbell, USA) installed on three soil profiles in the upslope, middle slope and downslope of the plots with a frequency of 20 min. Each soil profile included eight depths, that is, 20, 40, 60, 80, 130, 180, 230 and 280 cm.

We collected soil water, rainwater samples and subsurface flow samples for three typical storm events (April 11, April 24, June 10, 2021). The rainfall intensities of the three storm events were 1.1 mm h⁻¹, 1.3 mm h⁻¹ and 1.9 mm h⁻¹ with the rainfall amount of 26.6 mm, 30.5 mm, and 32.9 mm, respectively. We chose these three rainfall events for the following reasons. First, the median rainfall intensity was 1.1 mm h⁻¹ during the study hydrological year. The rainfall events with rainfall intensity between 1 mm h⁻¹ and 2 mm h⁻¹ accounted for 53.4% of the total rainfall events. Second, three selected storm events fell in the rainy seasons, and generated sufficient subsurface flow and accessed to obtain old water for analysis. Furthermore, three selected storm events had the similar rainfall amounts but different rain intensities, which was conducive to focus on the research purposes.

As the flow occurred, subsurface flow samples were collected hourly at three depths (30, 60 and 90 cm) in the plot until the flow ended. Pre-event soil water was collected by hydrophilic porous ceramic cups, which were installed on each soil profile of the upslope, middle slope and downslope of the plots. Hydrophilic porous ceramic cups were connected to zero-tension soil lysimeters via polyethylene pipes. The pressure was maintained at 75 kPa during the sampling process. Due to the low SWC before rainfall, the time for which pressure was maintained could be appropriately prolonged.

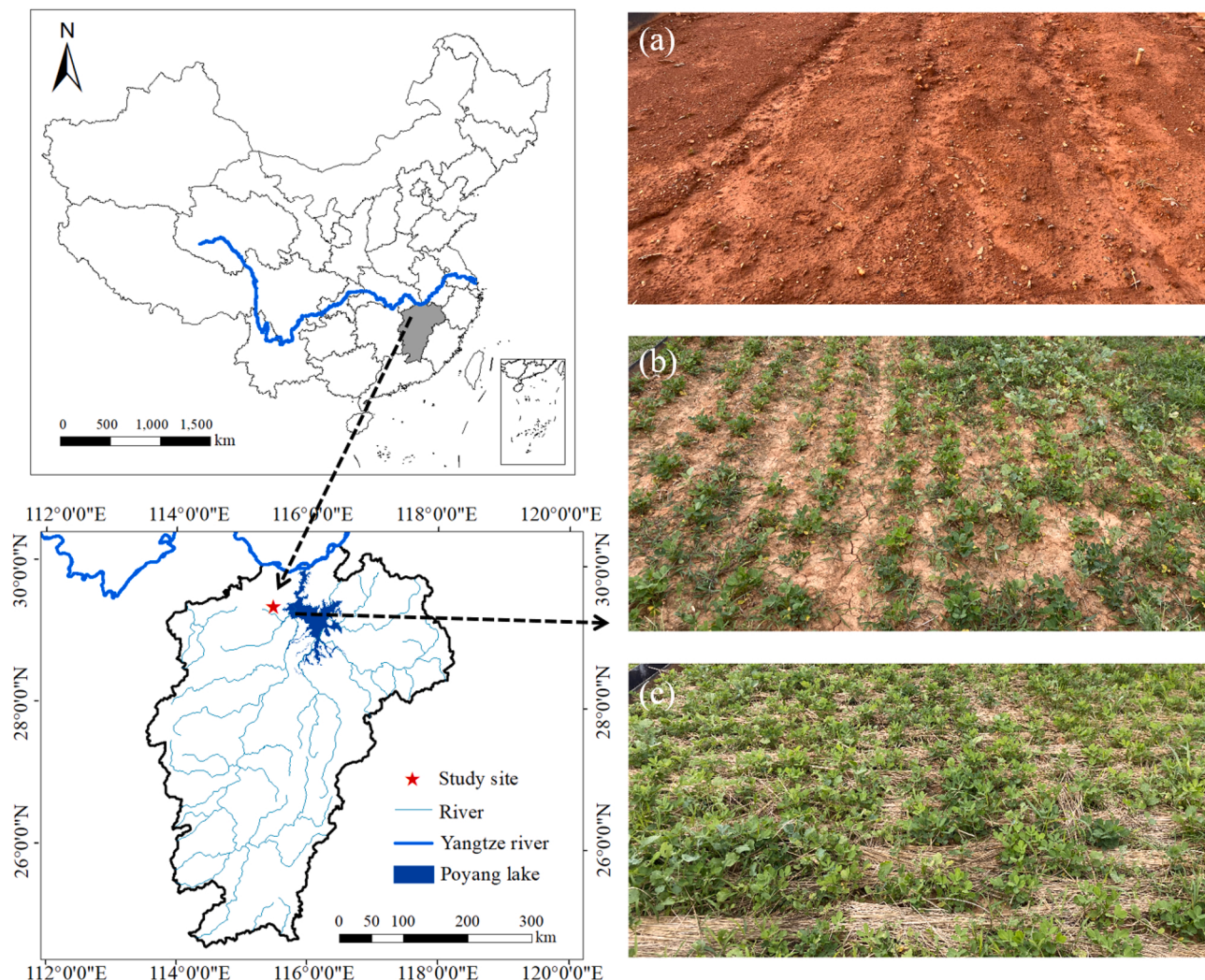


Fig. 1. The experiment was conducted in the red soil hilly region of southern China. The three pictures on the right show the sloping experimental plots with different tillage regimes, including bare land (a), no-tillage (b) and straw mulching (c).

Table 1
Soil physicochemical properties of the sloping experimental plots.

Farming practices	Depth (cm)	Soil organic matter (g kg^{-1})	pH	Cation exchange capacity (mol kg^{-1})	Soil particle size distribution		
					Clay (%)	Silt (%)	Sand (%)
bare land	0-20	9.73	4.66	8.69	36.46	54.70	8.84
	20-40	5.99	4.74	8.82	34.48	52.73	12.79
	40-60	4.52	5.08	8.30	34.39	54.62	10.99
no-tillage	0-20	12.90	6.14	9.60	30.35	58.68	10.97
	20-40	6.56	4.96	7.79	36.44	56.69	6.87
	40-60	3.64	4.99	9.47	30.41	58.80	10.79
straw mulching	0-20	14.91	5.55	9.60	28.36	62.79	8.85
	20-40	7.84	4.81	8.30	30.96	59.87	9.17
	40-60	5.49	5.12	10.63	26.85	68.16	4.98

A polyethylene bottle and funnel with a 15 cm diameter were used to collect rainwater. A plastic ball was placed in a funnel to prevent evaporation (Wang et al., 2017). Two kinds of rainwater samples were collected in our experiments. One kind was intended to collect rainwater from the entire storm. A total of 48 rainwater samples were collected from April to September 2021 to linearize the local meteoric water line (LMWL). The other kind was intended to collect hourly rainwater samples during the storm. When the precipitation ended, rainwater samples were immediately collected in a polyethylene bottle, sealed with parafilm, and refrigerated at 4 °C for stable isotope analysis.

2.3. Isotopic analyses

The isotopic measurements of water samples were determined using a liquid water isotope analyzer (L2140-i, Picarro, USA). The analytical precision of the measured liquid water was $\pm 0.1\text{\textperthousand}$ for $\delta^{2\text{H}}$ and $\pm 0.025\text{\textperthousand}$ for $\delta^{18}\text{O}$. The isotopic compositions in the water samples were expressed as follows:

$$\delta X = \left(\frac{R_{sample}}{R_{standard}} - 1 \right) \times 1000\% \quad (1)$$

where X represents 2H or ^{18}O , R_{sample} and $R_{standard}$ represent $^2H/^{1H}$ or $^{18}O/^{16}O$ ratio of the sample and standard, respectively. The standard is Vienna Standard Mean Ocean Water. Measurement of the degree of disequilibrium isotope effects used the deuterium excess parameter (d -excess) (Sprenger et al., 2016a).

$$d - \text{excess} = \delta^2H - 8 \times \delta^{18}O \quad (2)$$

2.4. Water source partitioning for subsurface flow

The isotopic values of soil water at different depths were weighted using the SWC of each depth. The isotopic compositions in rainwater were weighted using the incremental intensity mean (McDonnell et al., 1990).

$$\delta^2H \text{ or } \delta^{18}O, \text{mean} = \frac{\sum_i I_i \delta_i}{\sum_i I_i} \quad (3)$$

where I_i represents the average rainfall intensity per hour during each storm event, and δ_i is the δ value of rainwater collected in each hour. n is the total number of rainwater samples collected during each storm event.

Water source partitioning for subsurface flow was estimated by the Bayesian isotope mixing model MixSIAR (version 3.1.7) (Stock et al., 2018; Wang et al., 2019b). The contributions of new water and old water to subsurface flow were calculated for each storm event. In the model, the δ^2H and $\delta^{18}O$ values of subsurface flow were regarded as the mixture data, while the δ^2H and $\delta^{18}O$ values of rainwater and pre-event soil water at different slope positions were regarded as the source data. The discrimination data in the model were set to 0. Markov chain Monte Carlo (MCMC) was applied to simulate the posterior convergence of all variables. The length of MCMC was first set to 'long' (chain length = 300,000; burn = 200,000; thin = 100; chains = 3). Gelman-Rubin and Geweke diagnosis tests were used to determine whether the posterior distribution simulation converged, and then adjusted MCMC parameter settings until the model converged. The median results of the model output were taken as the contribution proportions of different water sources to subsurface flow. To facilitate the subsequent analysis and comparison, pre-event water from different soil depths were combined into three layers. All of the statistical analyses were conducted in R (v.3.4.4, R Core Team, 2018).

3. Results

3.1. Precipitation isotopic composition

The total precipitation in the study year was 1437.8 mm, which mainly occurred from April to July, accounting for 61.12% of the total precipitation. Compared with the multiyear (2010–2017) average (1590.2 mm), the precipitation amount in 2021 decreased by 9.58%. The monthly variation was consistent with that of the multiyear average (Fig. 2a). The $\delta^{18}O$ ranged from -11.38‰ to -1.12‰ , with an average of -5.58‰ , and δ^2H ranged from -86.58‰ to 17.01‰ , with a mean value of -32.29‰ . The isotopic compositions of rainwater varied with seasons. From March to September, the isotopic ratios of rainwater became depleted, and the dispersion degree increased (Fig. 2b). Compared with soil water and subsurface flow, the isotopic values in rainwater showed the widest variation range, and the mean isotopic value was the most depleted (Fig. 3). The isotopic compositions for the majority of subsurface flow were in the range of rainwater and soil water, suggesting that the subsurface flow was derived from rainwater and soil water. The relationship between $\delta^{18}O$ and δ^2H for the rainwater

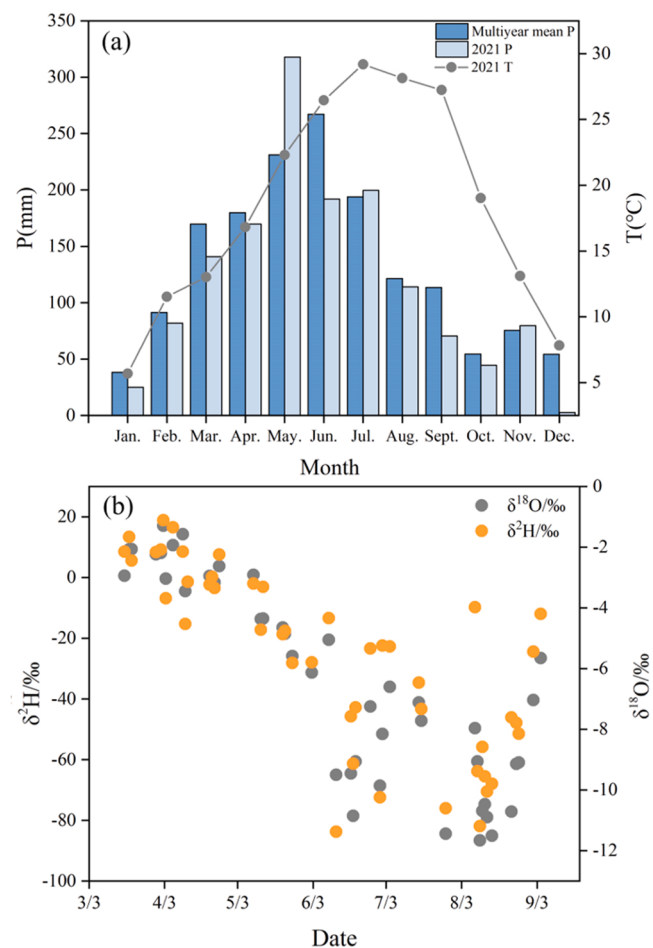


Fig. 2. The temporal distribution of precipitation, air temperature and isotopic compositions in rainwater: (a) the monthly variation in multiyear precipitation (2010–2017), temperature and precipitation in 2021; (b) the distribution of isotopic compositions ($\delta^{18}O$ and δ^2H) in rainwater during the study period.

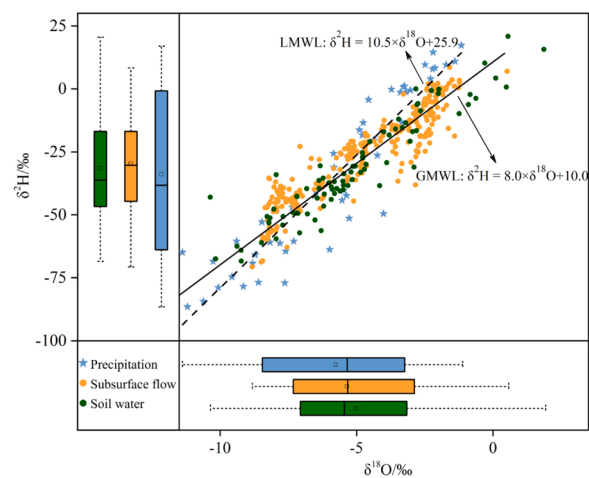


Fig. 3. Dual isotope and box plots showing the isotopic values (δ^2H and $\delta^{18}O$) of rainwater, soil water and subsurface flow, as well as LMWL. LMWL represents the local meteoric water line (dashed line, $\delta^2H = 10.5 \delta^{18}O + 25.9$, $R^2 = 0.89$, $P < 0.01$, which was based on the stable isotope data of rainwater from March to September 2021), and GMWL is the global meteoric water line (solid line, $\delta^2H = 8 \delta^{18}O + 10$).

samples was shown in Fig. 3. The LMWL was expressed as the equation $\delta^2\text{H} = 10.5 \delta^{18}\text{O} + 25.9$, $R^2 = 0.89$. The slope and intercept of the LMWL were larger than those of the global meteoric water line (GMWL: $\delta^2\text{H} = 8 \delta^{18}\text{O} + 10$), indicating the warm and humid climate characteristics of the monsoon region in this study area.

3.2. Variation in soil moisture and its isotopic compositions

The SWC of the experimental plots showed spatial heterogeneity. The average SWC on the upslope, middle slope and downslope of the plots was 33.27%, 30.94% and 32.74%, respectively. In the vertical direction, the SWC increased with depth and tended to saturate (Fig. 4). The SWC changed significantly during rainfall. At the beginning of rainfall, the SWC at 0–40 cm increased rapidly. With the infiltration of rainwater, the SWC at 40–130 cm began to increase, and the lag effect became more significant with increasing depths. When the storm ended, the SWC at 0–40 cm decreased gradually, while the SWC at 130–280 cm was higher and changed only slightly during rainfall (Fig. 4). The SWC of different tillage regimes showed specific changes during rainfall. After three storm events, the SWC of 0–40 cm in the bare land plot, the no-tillage plot and the straw mulching plot increased by an average of 16.97%, 17.90% and 21.53%, respectively. The increase in the SWC at 40–130 cm was smaller than that in the shallow soil layer, and the response time was longer with increasing soil depths (Fig. 4). For the 130–280 cm soil layers, the SWC remained relatively stable before and after storms, and the SWC in the no-tillage plot was the highest, reaching 41.09% (Fig. 4b).

The $\delta^{18}\text{O}$ and $\delta^2\text{H}$ of soil water ranged from –7.06‰ to –3.16‰, and –46.71‰ to –16.85‰, with average values of –5.03‰ and –31.49‰, respectively (Fig. 3). The isotopic compositions of the soil water before the storm changed along the soil profile (Fig. 5). Soil water isotopes showed a trend of first decreasing and then increasing with depths. For most soil profiles, the isotopic ratios in soil water were depleted at 0–130 cm and enriched at 130–280 cm with increasing depths. The average value of *d*-excess before storms was 8.44 and increased by 10.31% after rainfall, but both were lower than the global average *d*-excess value of 10, indicating that the evaporation cycle of water vapor was not significant.

The isotopic compositions of soil water changed significantly along the profile after storms. For most soil profiles, the distribution of isotopic values in deep soil water were similar before and after storms. The variation of shallow soil water isotopic values for experimental plots with different farming practices were different before and after storms (Fig. 5). In addition, most of the $\delta^{18}\text{O}$ and $\delta^2\text{H}$ in shallow soil water after storms were close to those of rainwater, whereas this pattern was not the case for deep soil water (Fig. 5). For example, the isotopic values in soil water at 130 cm depth in the no-tillage plot in the storm on June 10 deviated from rainwater isotopes (Fig. 5b). The isotopic compositions for soil water of the straw mulching experimental plot that occurred in the April 11 storm showed a similar pattern at 80–230 cm after storms (Fig. 5c).

3.3. Identification water sources of subsurface flow

The MixSIAR model predicted that the average contribution of old water to subsurface flow of the three experimental plots was 68.17% during the storm on April 11 (Fig. 6). The proportion of new water to subsurface flow for the no-tillage plot decreased with increasing depth, and the average proportions of new water to subsurface flow from 0–30 cm, 30–60 cm and 60–90 cm were 63.12%, 44.03% and 25.62%, respectively (Figs. 6a, 6b and 6c). In addition, the average proportional contributions of new water to the subsurface flow from 0–30 cm in the bare land plot and the straw mulching plot were 21.10% and 39.15%, respectively. (Figs. 6d and 6f).

The proportional contributions of old water to the subsurface flow during the April 24 storm were the largest of the three storms, with an

average of 88.70%. The subsurface flow at 0–30 cm for the straw mulching plot was primarily derived from old water (98.93%) (Fig. 7d). The proportions of new water to subsurface flow during the storm events were dynamic. For the no-tillage plot, almost all subsurface flow from 0–30 cm came from old water (99.70%) within 9 h of runoff generation, and then the percentage of new water increased to 63.76% (Fig. 7a). The subsurface flow from 30–60 cm showed similar changes in water sources, but the fractions of new water were low (13.88%) (Fig. 7b). For the subsurface flow from 60–90 cm, the proportions of new water in the experimental plot remained relatively stable during the whole rainfall process (Fig. 7c). For most of the subsurface flow, the old water was dominated by downslope. The old water mainly came from the middle slope for the subsurface flow from 30–60 cm in the no-tillage plot and the straw mulching plot (Figs. 7b and 7e).

The average proportion of new water to subsurface flow for the three experimental sloping plots during the storm on June 10 was 22.91% (Fig. 8). The contributions of new water to subsurface flow from 0–30 cm of the no-tillage plot first increased and then decreased with the progress of rainfall (Fig. 8a). For the subsurface flow from 60–90 cm of the no-tillage plot, the fractions of old water from the downslope were approximately 75% (Fig. 8c). However, the proportion of new water to subsurface flow remained stable in some experimental plots with different tillage regimes, such as the subsurface flow from 60–90 cm in the no-tillage plot, the subsurface flow from 30–60 cm for the straw mulching plot and the subsurface flow from 0–30 cm in the bare land plot (Figs. 8c, 8e and 8f).

4. Discussion

4.1. Infiltration and mixing processes of new and old water

The mixing degree of new and old water affects the distribution of SWC and its isotopic compositions at the slope scale (Liao et al., 2017; Xiao et al., 2020b). SWC and isotopic ratios in soil water exhibit spatial heterogeneity, which is controlled by evaporation and rainwater infiltration (Chen et al., 2022; Yang et al., 2020; Zhang et al., 2021). Our results indicated that the SWC increased with soil depth and the $\delta^{18}\text{O}$ and $\delta^2\text{H}$ of soil water were enriched in shallow and deep layers (Figs. 4 and 5). The reason is that the soil water in the shallow layer was lost by evaporation, and most of the water infiltrated downward under the force of gravity (Sprenger et al., 2016a). The isotopic compositions of shallow soil water became enriched by evaporation (Jiang et al., 2021). However, the SWC of deep soil tends to be stable due to the lower impact of rainfall pulses and evaporation, and the isotopic values in deep soil water were enriched which may be due to the long-term retention of old water (Oerter and Bowen, 2019).

Mixing processes of new and old water were complicated during storm events. Rainwater entered the pores first and immediately mixed with the previous remaining water inside the soil (Sayama and McDonnell, 2009). As rainfall progressed, the mixed water moved into larger pores and downward at a faster rate. A similar phenomenon was observed in the previous study (Dahlke et al., 2012). Zhao et al. (2013) reported that soil macropores and mudstone fractures were important channels for water movement in soil. The input of rainwater led to the initial sharp increase in SWC. However, the lag effect of SWC from the shallow layer to the deep layer gradually became significant because the infiltration rate of soil water slowed with increasing depth (Fig. 4). There were significant differences in $\delta^{18}\text{O}$ and $\delta^2\text{H}$ between rainwater and soil water (Fig. 5), and the input of rainwater significantly changed the isotopic compositions of soil water. The variation in the isotopic values of soil water before and after storms indicated that rainwater and soil water mixed to different degrees, which may be related to rainfall characteristics, soil texture and pores (Sun et al., 2019).

The movement mechanisms of soil water had piston flow and preferential flow, and the dominant mechanisms changed over time and spatial locations (Zhao et al., 2016). For the red soil hilly slopes, we

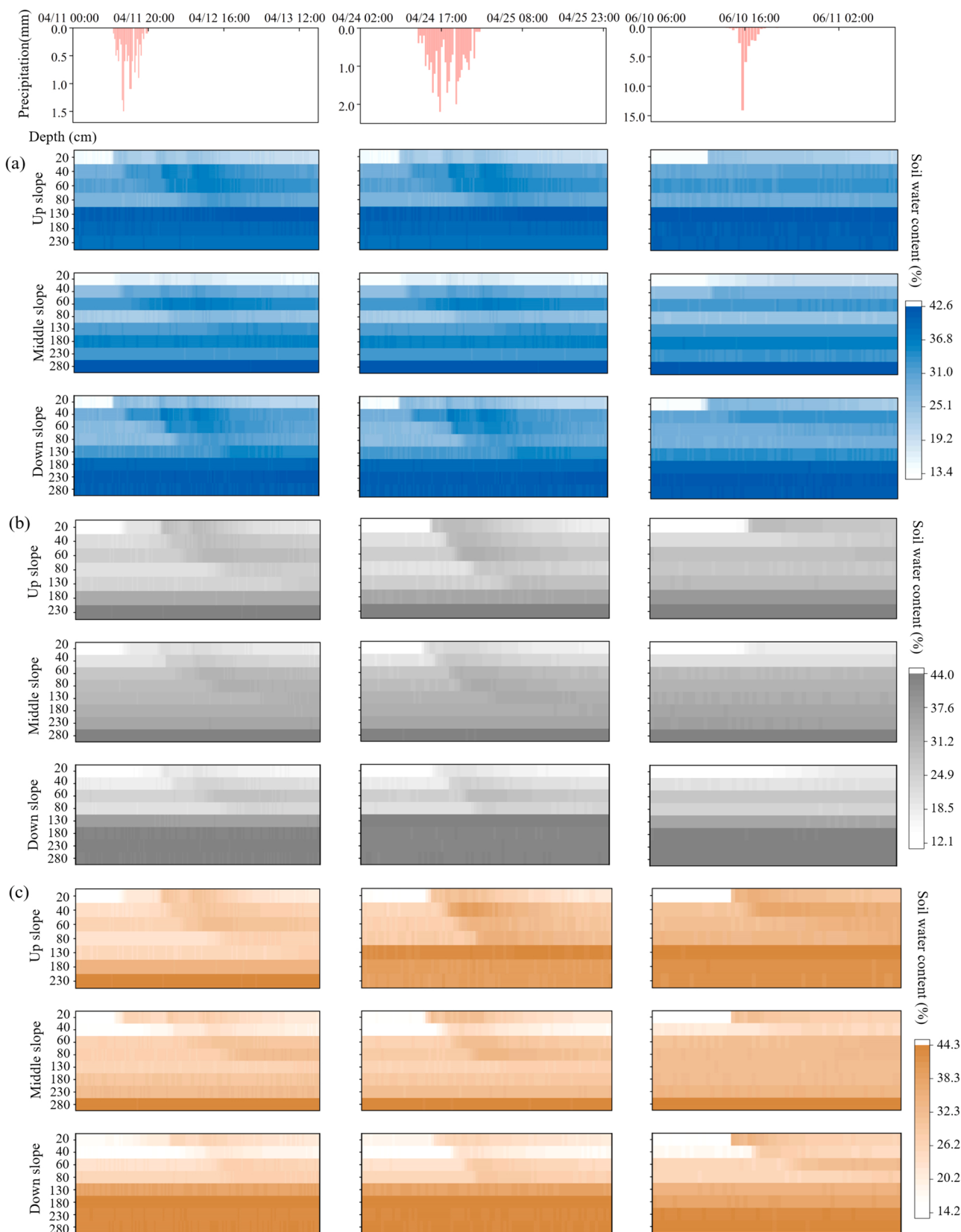


Fig. 4. Rainfall intensity of three storm events on 11 April, 24 April and 10 June and the variations in SWC in sloping experimental plots under three tillage regimes: (a) bare land; (b) no-tillage; and (c) straw mulching. The heatmap shows the SWC of each slope plot at different depths at three locations: upper slope, middle slope and lower slope.

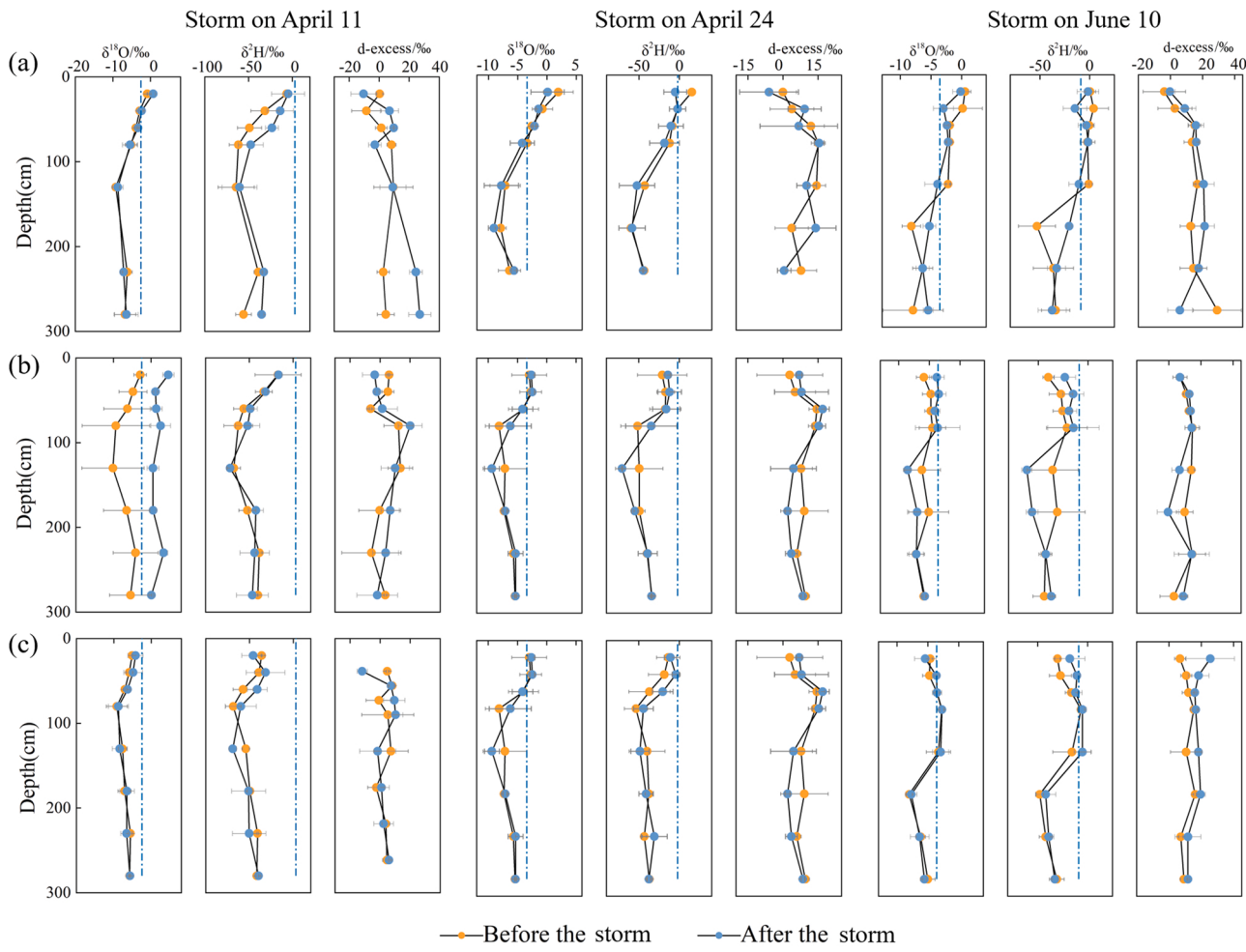


Fig. 5. Distribution of $\delta^2\text{H}$ and $\delta^{18}\text{O}$ of soil water in sloping experimental plots, (a) bare land; (b) no-tillage; (c) straw mulching along the soil profile before and after three storm events. The dashed lines indicate the weighted mean isotopic composition of rainwater for each storm.

found that piston flow and preferential flow coexisted during the process of soil water movement (Fig. 9). Comparing the $\delta^{18}\text{O}$ and $\delta^2\text{H}$ of soil water along the soil profile before and after storm events, not all the isotopic compositions of soil water after storms were close to those of rainwater, which provided evidence of piston flow (Pu et al., 2020). The $\delta^{18}\text{O}$ and $\delta^2\text{H}$ of soil water from 130–180 cm depth in the no-tillage plot in the June 10 storm deviated from the isotopic ratios of the rainwater (Fig. 5b). The main reason was that soil water in the upper layer migrated to 130–180 cm in the form of piston flow and affected its isotopic compositions. In addition, the outcomes of water source partitioning in subsurface flow confirmed the existence of piston flow. For example, for the no-tillage plot on the April 24 storm event, the subsurface flow from 0–30 cm in the first 9 h of the storm was dominated by old water (99.70%) and then converted to new water (63.76%) (Fig. 7a). This phenomenon can be explained by the fact that at the beginning of rainfall, old water was pushed downward by new water and large amounts of old water flowed out. In the later period of storm, with the establishment of hydrological connectivity along the soil profile, parts of the flow path channel were activated (Xiao et al., 2022). New water continuously displaced the pre-existing old water and became the main water source of subsurface flow in the soil profile (Li et al., 2017). Numerous studies have shown that preferential flow is caused by the presence of large pores, decaying plant roots (Zhu et al., 2019), worm holes and rocks in the soil (Chen et al., 2021). In our study, peanuts were planted in the no-tillage plot and straw mulching plot during the study period, and the roots of peanuts were mainly distributed in the 0–30 cm soil layer. Through high-frequency soil moisture monitoring

data, we found that the SWC of deep soil tended to increase earlier than that of shallow soil during storm events (Fig. 4), which may be due to the rapid downward infiltration of rainwater through large pores (Jiang et al., 2020). Additionally, we observed that a certain proportion of new water was involved in the generation of subsurface flow in deep soil (Fig. 6–8). These results indicated that preferential flow was also a non-negligible form of soil water movement at the hillslope scale. The generation and development of preferential flow are affected by various environmental factors, which have obvious regional characteristics (Nimmo, 2021). Zheng et al. (2019) found that the dominant pattern of soil water movement in the North China Plain was piston flow in normal years but changed from piston flow to preferential flow after extreme precipitation in the rainy season.

4.2. Generation and water sources partitioning of subsurface flow

The generation of subsurface flow is closely related to soil properties and depends on a relatively impermeable layer (Kidron, 2021; Gray et al., 2016). Due to the heavy soil texture, gravity and long-term compaction of tillage, there were spatial differences in the water permeability of red soil, which were conducive to the generation of subsurface flow (Ma et al., 2022). In our study, the generation of subsurface flow in sloping experimental plots under different tillage regimes showed different patterns. The proportion of clay particles in the bare land plot was the highest (Table 1), and there was crust on the surface, which hindered the infiltration of rainwater (De Rouw and Rajot, 2004). Therefore, the generation of subsurface flow was only observed from

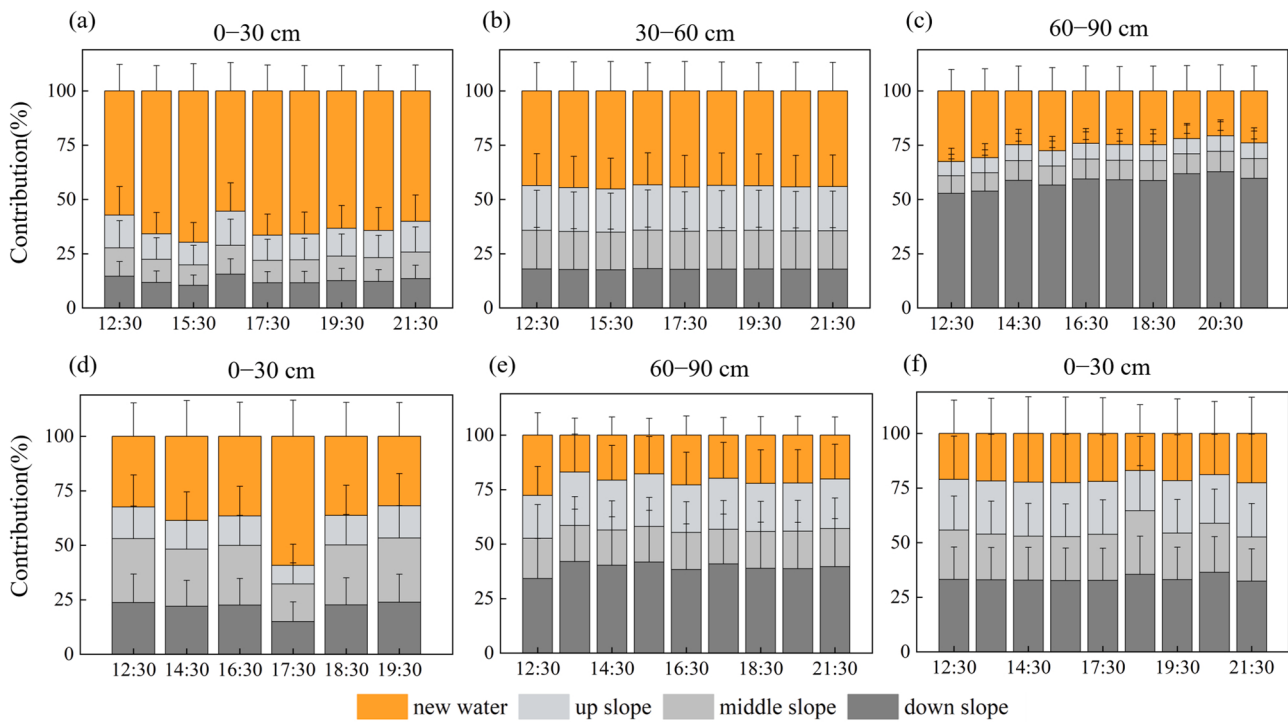


Fig. 6. The contributions of various water sources to subsurface flow during the April 11 storm. Yellow and gray represent new water and old water at different slope positions, respectively. no-tillage: (a) (b) (c); straw mulching: (d) (e); bare land: (f). Error bars represent standard deviation.

0 – 30 cm (Figs. 6f, 8g, and 9f). A previous study also demonstrated that bare land generated the lowest subsurface flow rate compared with grassland cover and litter cover at the runoff plot in the red soil region of China (Liu et al., 2016). The straw mulching plot prolonged the infiltration time and reduced evaporation of the soil surface, facilitating the generation of subsurface flow (Garba et al., 2022; Xiao et al., 2019). However, surface runoff produced by rainfall is dominate when rainfall intensity is greater than soil infiltration rate. Therefore, we did not observe the generation of subsurface flow in deep soil layer in the straw mulching plot (e.g., the June 10 storm). Compared to tillage, no-tillage preserved the original well-structured paths for water movement in the soil and increased the number of macropores, promoting rainwater infiltration (Shakoor et al., 2021). The average contribution proportions of old water to subsurface flow in the 11 April, 24 April and 10 June storms were 68.17%, 88.74% and 77.09%, respectively, indicating that old water was the main water source of subsurface flow. This result was consistent with previous studies (Sayama and McDonnell, 2009; Sang et al., 2022). The variation of water source partitioning for subsurface flow among three storm events indicated that rainfall conditions may affect the water sources of subsurface flow at the slope scale. This is mainly attributed to the distinct hydrological connectivity on the slope under various rainfall conditions, resulting in different water residence time and hydrological connectivity maintenance time on the soil profile (Xiao et al., 2022). Furthermore, the proportion of new water decreased with increasing soil depth because the deep soil had less rainwater recharge and a higher antecedent SWC.

The water sources of subsurface flow showed a dynamic change during rainfall. For the 24 April storm, the shallow subsurface flow from 0 – 30 cm usually derived out the old water in the early stage of rainfall (Pu et al., 2020). As more rainwater was input, the new water fully mixed with the old water, and its contribution proportion increased gradually (Figs. 6, 7, and 8). The subsurface flow from 30 – 60 cm showed similar changes, but the fluctuation was smaller. The water source from 60 – 90 cm was relatively stable and needed to be connected with the macropores in the soil (Zhao et al., 2016). At the beginning of the storm, the mixing of new water and old water was

limited (Klaus and McDonnell, 2013). The large pores in the soil formed preferential channels which allowed new water to participate in the generation of subsurface flow, but these channels were not a continuous network due to the low hydrological connectivity between pores, so their transport efficiency was limited (Zhao et al., 2016). In the later stage of the storm, the recharge of new water increased, while the hydrological connectivity between the channels increased, more old water was connected to the flow generation network, and the two processes maintained a dynamic balance (Fig. 9). Some previous model simulation results showed that old water was still the main water sources of subsurface flow even when preferential flow was dominant (Dusek and Vogel, 2018; Adyel et al., 2016). However, these studies did not give a detailed change process of the water sources during the storm.

4.3. Implications for water and land management

Although there is abundant precipitation in the area of southern China, the rainfall distribution is uneven. The rainy season overlaps with strong evaporation and high temperature periods, which can easily cause seasonal droughts (Hao et al., 2018). This seasonal drought has a severe impact on the agricultural ecosystem, such as reducing crop yield and available water resources (Hao et al., 2018). The frequency and magnitude of seasonal droughts are likely to increase further, as predicted by climate models and meteorological observations (Lu et al., 2017). Rational farming practices are an important way to deal with seasonal drought in agricultural ecosystems. Previous studies showed that farming practices improved soil structure by changing the organic carbon content and soil microbial communities in the soil profile (Hu et al., 2021; Bai et al., 2018), thereby promoting the soil infiltration capacity and water storage capacity. Our results showed that farming practices affected soil water movement and water sources of subsurface flow at a hillslope scale. New water contributed the largest proportions to subsurface flow from 0 – 30 cm in the experimental plots with no-tillage during the storm events, compared with bare land and conventional tillage experimental plots (Figs. 6, 7, and 8). The SWC in the no-tillage plot for deep soil (130 – 280 cm) was the highest (41.09%)

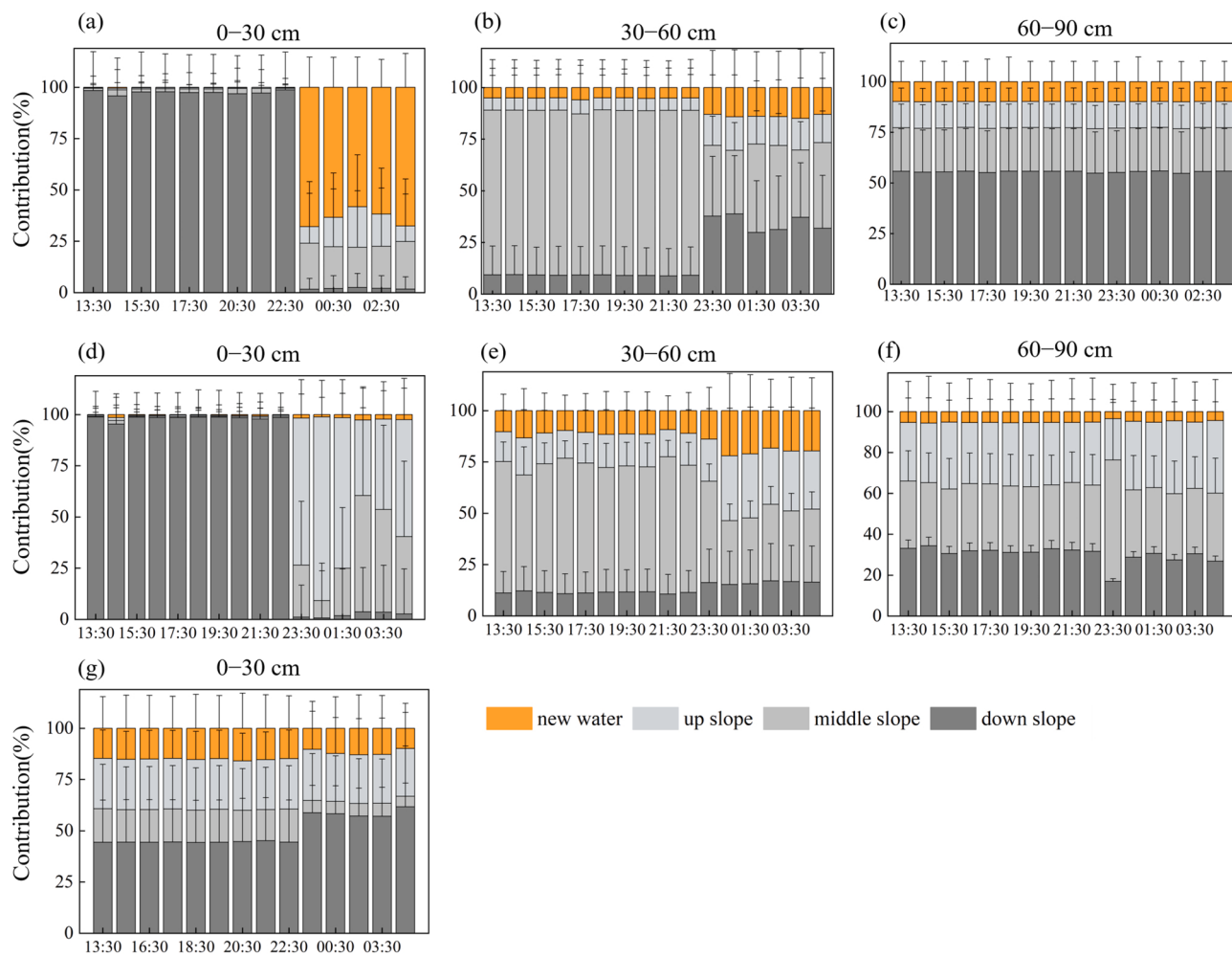


Fig. 7. The contributions of various water sources to subsurface flow during the April 24 storm. Yellow and gray represent new water and old water at different slope positions, respectively. no-tillage: (a) (b) (c); straw mulching: (d) (e) (f); bare land: (g). Error bars represent standard deviation. (For interpretation of the references to colour in this figure legend, the reader is referred to the web version of this article.)

among the different farming practices after storm events (Fig. 4). These results suggested that no-tillage was more conducive to rainwater infiltration and water storage, which would be beneficial for agricultural systems in seasonal drought. Sun et al. (2015) also found that no-tillage could significantly reduce surface runoff through an integrated analysis of global field plot experiments. In addition, the SWC of shallow soil water in the straw mulching plot increased by an average of 21.53% after three storm events (Fig. 4), and more old water contributed to the subsurface flow, indicating that more rainwater entered into the soil to drive away old water. Mulching, such as vegetative residues and biological geotextiles, could effectively reduce soil erosion rates and runoff coefficients, and increase soil water storage capacity by increasing infiltration, inhibiting evaporation, and reducing runoff velocity (Prosdocimi et al., 2016; Tu et al., 2021). Therefore, no-tillage and mulching may be better methods of water and land management, which is beneficial to the sustainable development of agro-environmental systems. However, the implementation of water and land management practices should take into account the wishes of local residents and the economic costs.

5. Conclusion

To reveal the soil water movement and water sources of subsurface flow at a hillslope scale with different farming practices, the $\delta^{18}\text{O}$ and $\delta^2\text{H}$ of soil water before and after storm events were investigated, and

water sources of subsurface flow were determined during three storm events (11 April, 24 April and 10 June storms) combined with the MixSIAR model. The results showed that the isotopic compositions in soil water showed spatial heterogeneity due to the impact of rainfall infiltration, depending on the different degrees of mixing between new and old water. Both piston flow and preferential flow were observed on red soil hillslopes, and the dominant mode changed during rainfall depending on the antecedent SWC. In the bare land plot, subsurface flow was only observed in the 30 cm soil layer, which was mainly derived from old water (77.61%). The fractions of new water to subsurface flow from 0–30 cm for the no-tillage, bare land, and straw mulching plots were 46.60%, 22.39%, and 15.70%, respectively, suggesting that farming practices influenced soil movement and water sources of subsurface flow. In the three storm events, the average contribution proportions of old water to subsurface flow were 68.17%, 88.70% and 77.09%, respectively, indicating that subsurface flow was mainly derived from old water. The average contribution of new water to the subsurface flow decreased with increasing soil depth and changed dynamically during rainfall.

In this study, soil water movement and water sources of subsurface flow on a hillslope with red soil were elucidated by high-frequency hydrological monitoring and stable isotope technique. Our results enrich the understanding of the generation mechanisms of subsurface flow during storms and provide a scientific basis for the selection of agricultural water and land management in the red soil region. This

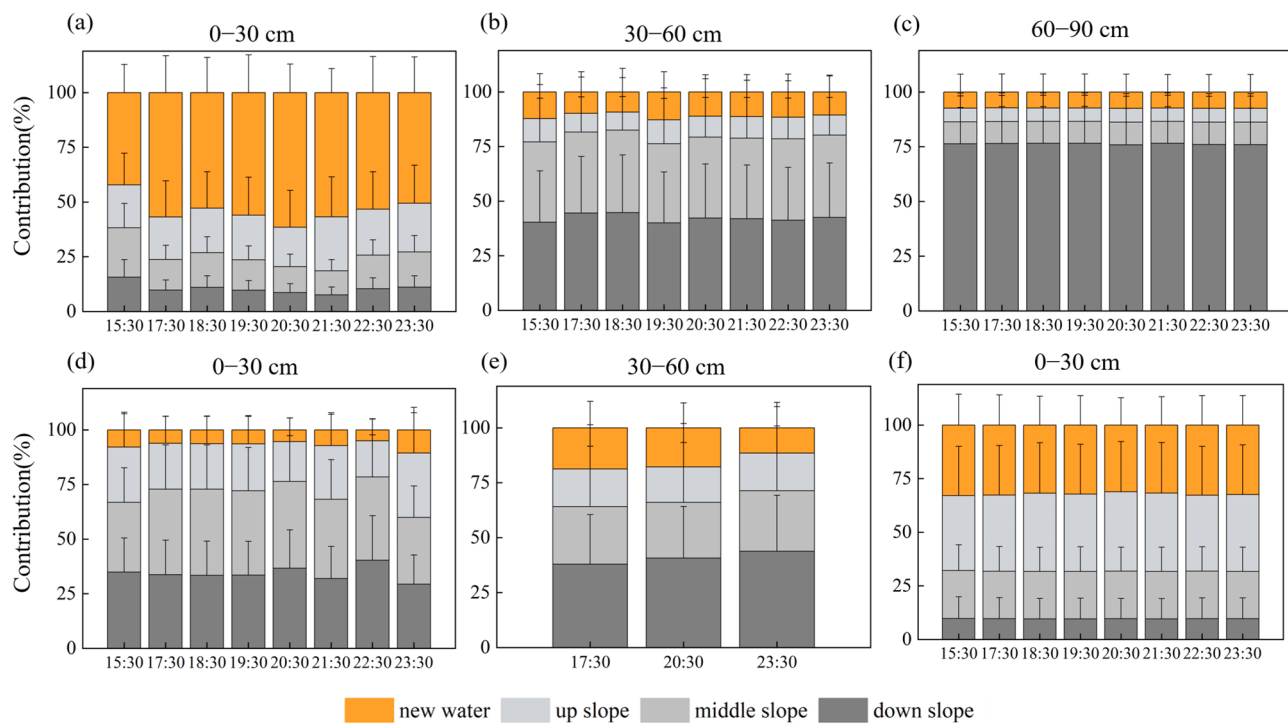


Fig. 8. The contributions of various water sources to subsurface flow during the June 10 storm. Yellow and gray represent new water and old water at different slope positions, respectively. no-tillage: (a) (b) (c); straw mulching: (d) (e); bare land: (f). Error bars represent standard deviation.

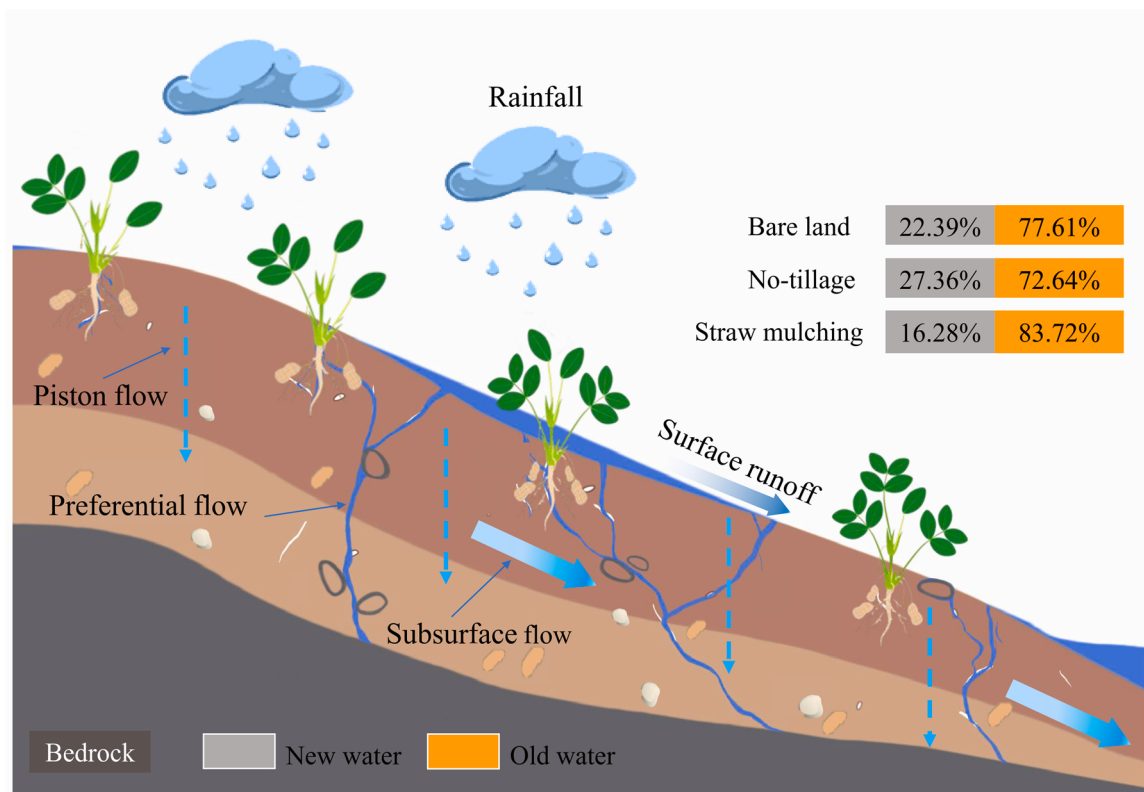


Fig. 9. Sketch map of soil water movement during rainfall. Gray and orange represent the contributions of new water and old water to subsurface flow, respectively. (For interpretation of the references to colour in this figure legend, the reader is referred to the web version of this article.)

study provides a useful method to identify the water source partitioning of subsurface flow at the slope scale and crucial guidance for the management of soil and water resources. However, we investigated only the

water sources of subsurface flow for three storm events and three different farming practices on the slopes. Multiscale monitoring for more storm events under different soil type zones should be investigated in

future studies. Additionally, we can explore the generation and water source partitioning of subsurface flow in various vegetation community types, such as mixed shrub-crop types and tree-shrub types. Furthermore, isotope *in situ* real-time monitoring technology combined with hydrological process models may bring new breakthroughs to this topic of research.

Declaration of Competing Interest

The authors declare that they have no known competing financial interests or personal relationships that could have appeared to influence the work reported in this paper.

Data availability

Data will be made available on request.

Acknowledgments

This research was financially supported by National Natural Science Foundation of China (NSFC 42107354, 41930755), the Open Fund from Jiangxi Provincial Key Laboratory of Soil Erosion and Prevention (KFJJ202005, 2021SKTR01), the Project of Hydraulic Science and Technology of Jiangxi Province (202124ZDKT24), the China Postdoctoral Science Foundation (2019M662668). We are grateful to Zijing Zhang, Lijie Zhang, Chengshuai Liu, Xiaodie Hu and Yingping Xiao for the assistance in the field experiments.

References

- Adyel, T.M., Oldham, C.E., Hipsey, M.R., 2016. Stormwater nutrient attenuation in a constructed wetland with alternating surface and subsurface flow pathways: event to annual dynamics. *Water Res.* 107, 66–82. <https://doi.org/10.1016/j.watres.2016.10.005>.
- Bah, H.D., Zhou, M.H., Ren, X., Hu, L., Dong, Z.X., Zhu, B., 2020. Effects of organic amendment applications on nitrogen and phosphorus losses from sloping cropland in the upper Yangtze River. *Agric., Ecosyst. Environ.* 302, 107086 <https://doi.org/10.1016/j.agee.2020.107086>.
- Bai, Z., Caspari, T., Gonzalez, M.R., Batjes, N.H., Mäder, P., Bünenmann, E.K., Goede, R.D., Brussaard, L., Xu, M., Ferreira, C.S., Reintam, E., Fan, H., Mihelić, R., Glavan, M., Tóth, Z., 2018. Effects of agricultural management practices on soil quality: a review of long-term experiments for Europe and China. *Agric., Ecosyst. Environ.* 265, 1–7. <https://doi.org/10.1016/j.agee.2018.05.028>.
- Beyer, M., Kühnhammer, K., Dubbert, M., 2020. In situ measurements of soil and plant water isotopes: a review of approaches, practical considerations and a vision for the future. *Hydrol. Earth Syst. Sci.* 24 (9), 4413–4440. <https://doi.org/10.5194/hess-24-4413-2020>.
- Carpena, R.M., Lauvernet, C., Carluer, N., 2018. Shallow water table effects on water, sediment, and pesticide transport in vegetative filter strips – Part 1: nonuniform infiltration and soil water redistribution. *Hydrol. Earth Syst. Sci.* 22 (1), 53–70. <https://doi.org/10.5194/hess-22-53-2018>.
- Chen, C., Zou, X., Singh, A.K., Zhu, X., Zhang, W., Yang, B., Jiang, X., Liu, W., 2021. Effects of hillslope position on soil water infiltration and preferential flow in tropical forest in southwest China. *J. Environ. Manag.* 299, 113672 <https://doi.org/10.1016/j.jenvman.2021.113672>.
- Chen, J., Xiao, H.B., Li, Z.W., Liu, C., Ning, K., Tang, C.J., 2020. How effective are soil and water conservation measures (SWCMs) in reducing soil and water losses in the red soil hilly region of China? A meta-analysis of field plot data. *Sci. Total Environ.* 735, 139517 <https://doi.org/10.1016/j.scitotenv.2020.139517>.
- Chen, M.Y., Shao, M.A., Wei, X.R., Li, T.C., Shen, N., Mi, M.X., Zhao, C.L., Yang, X., Gan, M., Bai, X., Li, A., 2022. Response of the vertical distribution of soil water and nitrogen in the 5 m soil layer to the conversion of cropland to apple orchards in the Loess Plateau, China. *Agric., Ecosyst. Environ.* 333, 107960 <https://doi.org/10.1016/j.agee.2022.107960>.
- Dahlke, H.E., Easton, Z.M., Lyon, S.W., Todd Walter, M., Destouni, G., Steenhuis, T.S., 2012. Dissecting the variable source area concept – Subsurface flow pathways and water mixing processes in a hillslope. *J. Hydrol.* 420–421, 125–141. <https://doi.org/10.1016/j.jhydrol.2011.11.052>.
- De Rouw, A., Rajot, J.L., 2004. Soil organic matter, surface crusting and erosion in Sahelian farming systems based on manuring or fallowing. *Agric., Ecosyst. Environ.* 104 (2), 263–276. <https://doi.org/10.1016/j.agee.2003.12.020>.
- Di Prima, S., Winiarski, T., Angulo-Jaramillo, R., Stewart, R.D., Castellini, M., Abou Najm, M.R., Ventrella, D., Pirastru, M., Giadrossich, F., Capello, G., Biddoccu, M., Lassabatere, L., 2020. Detecting infiltrated water and preferential flow pathways through time-lapse ground-penetrating radar surveys. *Sci. Total Environ.* 726, 138511 <https://doi.org/10.1016/j.scitotenv.2020.138511>.
- Dusek, J., Vogel, T., 2018. Hillslope hydrograph separation: the effects of variable isotopic signatures and hydrodynamic mixing in macroporous soil. *J. Hydrol.* 563, 446–459. <https://doi.org/10.1016/j.jhydrol.2018.05.054>.
- Fei, K., Deng, L.Z., Zhang, L.P., Sun, T.Y., Wu, Y.H., Fan, X.J., Dong, Y.Y., 2019. Lateral transport of soil total carbon with slope runoff and interflow: effects of rainstorm characteristics under simulated rainfall. *Catena* 179, 39–48. <https://doi.org/10.1016/j.catena.2019.03.030>.
- Garba, I.I., Fay, D., Apriani, R., Yusof, D.Y.P., Chu, D., Williams, A., 2022. Fallow replacement cover crops impact soil water and nitrogen dynamics in a semi-arid subtropical environment. *Agric., Ecosyst. Environ.* 338, 108052 <https://doi.org/10.1016/j.agee.2022.108052>.
- Gazis, C., Feng, X.H., 2004. A stable isotope study of soil water: evidence for mixing and preferential flow paths. *Geoderma* 119 (1–2), 97–111. [https://doi.org/10.1016/s0016-7061\(03\)00243-x](https://doi.org/10.1016/s0016-7061(03)00243-x).
- Gray, C.W., McDowell, R.W., Carrick, S., Thomas, S., 2016. The effect of irrigation and urine application on phosphorus losses to subsurface flow from a stony soil. *Agric., Ecosyst. Environ.* 233, 425–431. <https://doi.org/10.1016/j.agee.2016.09.040>.
- Hao, Z., Singh, V.P., Xia, Y., 2018. Seasonal drought prediction: advances, challenges, and future prospects. *Rev. Geophys.* 56 (1), 108–141. <https://doi.org/10.1002/2016RG000549>.
- Haruzi, P., Schmäck, J., Zhou, Z., van der Kruk, J., Vereecken, H., Vanderborght, J., Klotzsche, A., 2022. Detection of tracer plumes using full-waveform inversion of time-lapse ground penetrating radar data: a numerical study in a high-resolution aquifer model. e2021WR030110 *Water Resour. Res.* 58 (5). <https://doi.org/10.1029/2021wr030110>.
- Hu, X., Liu, J., Liang, A., Li, L., Yao, Q., Yu, Z., Li, Y., J, J., L, X., Wang, G., 2021. Conventional and conservation tillage practices affect soil microbial co-occurrence patterns and are associated with crop yields. *Agric., Ecosyst. Environ.* 319, 107534 <https://doi.org/10.1016/j.agee.2021.107534>.
- Huang, T.M., Ma, B.Q., Pang, Z.H., Li, Z., Li, Z.B., Long, Y., 2020. How does precipitation recharge groundwater in loess aquifers? Evidence from multiple environmental tracers. *J. Hydrol.* 583, 124532 <https://doi.org/10.1016/j.jhydrol.2019.124532>.
- Jasechko, S., Kirchner, J.W., Welker, J.M., McDonnell, J.J., 2016. Substantial proportion of global streamflow less than three months old. *Nat. Geosci.* 9 (2), 126–129. <https://doi.org/10.1038/ngeo2636>.
- Jiang, B.F., Cui, B., Wang, Y., Wang, Y., Li, D., Wang, L., Li, X., Li, X., Wang, G., 2021. Stable-isotope tracing of vadose-zone water transport in *Achnatherum splendens* grassland of the Qinghai Lake Basin, NE Qinghai-Tibet Plateau, China. *Catena* 200, 105088. <https://doi.org/10.1016/j.catena.2020.105088>.
- Jiang, X.J., Zakari, S., Wu, J.E., Singh, A.K., Chen, C.F., Zhu, X.A., Zhang, W.J., Liu, W.J., 2020. Can complementary preferential flow and non-preferential flow domains contribute to soil water supply for rubber plantation? *Ecol. Manag.* 461, 117948 <https://doi.org/10.1016/j.foreco.2020.117948>.
- Kidron, G.J., 2021. Comparing overland flow processes between semiarid and humid regions: Does saturation overland flow take place in semiarid regions? *J. Hydrol.* 593, 125624 <https://doi.org/10.1016/j.jhydrol.2020.125624>.
- Klaus, J., McDonnell, J.J., 2013. Hydrograph separation using stable isotopes: review and evaluation. *J. Hydrol.* 505, 47–64. <https://doi.org/10.1016/j.jhydrol.2013.09.006>.
- Li, Z., Chen, X., Liu, W., Si, B., 2017. Determination of groundwater recharge mechanism in the deep loess unsaturated zone by environmental tracers. *Sci. Total Environ.* 586, 827–835. <https://doi.org/10.1016/j.scitotenv.2017.02.061>.
- Liao, K.H., Lai, X.M., Zhou, Z.W., Zhu, Q., 2017. Applying fractal analysis to detect spatio-temporal variability of soil moisture content on two contrasting land use hillslopes. *Catena* 157, 163–172. <https://doi.org/10.1016/j.catena.2017.05.022>.
- Liu, Y.J., Yang, J., Hu, J.M., Tang, C.J., Zheng, H.J., 2016. Characteristics of the surface–subsurface flow generation and sediment yield to the rainfall regime and land-cover by long-term in-situ observation in the red soil region, Southern China. *J. Hydrol.* 539, 457–467. <https://doi.org/10.1016/j.jhydrol.2016.05.058>.
- Lu, H., Wu, Y., Li, Y., Liu, Y., 2017. Effects of meteorological droughts on agricultural water resources in southern China. *J. Hydrol.* 548, 419–435. <https://doi.org/10.1016/j.jhydrol.2017.03.021>.
- Ma, Y.C., Li, Z.W., Deng, C.X., Yang, J., Tang, C.J., Duan, J., Zhang, Z.W., Liu, Y.J., 2022. Effects of tillage-induced soil surface roughness on the generation of surface–subsurface flow and soil loss in the red soil sloping farmland of southern China. *Catena* 213, 106230. <https://doi.org/10.1016/j.catena.2022.106230>.
- McDonnell, J.J., Bonell, M., Stewart, M.K., Pearce, A.J., 1990. Deuterium variations in storm rainfall: Implications for stream hydrograph separation. *Water Resour. Res.* 26, 455–458. <https://doi.org/10.1029/WR026i003p00455>.
- Nazari, S., Ford, W.I., King, K.W., 2022. Impact of flow pathway and source water connectivity on subsurface sediment and particulate phosphorus dynamics in tile-drained agroecosystems. *Agr. Water Manag.* 269, 107641 <https://doi.org/10.1016/j.agwat.2022.107641>.
- Nimmo, J.R., 2021. The processes of preferential flow in the unsaturated zone. *Soil Sci. Soc. Am. J.* 85 (1), 1–27. <https://doi.org/10.1002/saj2.20143>.
- Oerter, E.J., Bowen, G.J., 2019. Spatio-temporal heterogeneity in soil water stable isotopic composition and its ecohydrologic implications in semiarid ecosystems. *Hydrolog. Process.* 33 (12), 1724–1738. <https://doi.org/10.1002/hyp.13434>.
- Pei, Y., Huang, L., Li, D., Shao, M.A., 2021. Characteristics and controls of solute transport under different conditions of soil texture and vegetation type in the water-wind erosion crisscross region of China's Loess Plateau. *Chemosphere* 273, 129651. <https://doi.org/10.1016/j.chemosphere.2021.129651>.
- Prosdocimi, M., Tarolli, P., Cerdà, A., 2016. Mulching practices for reducing soil water erosion: a review. *Earth-Sci. Rev.* 161, 191–203. <https://doi.org/10.1016/j.earscirev.2016.08.006>.

- Pu, H.M., Song, W.F., Wu, J.K., 2020. Using soil water stable isotopes to investigate soil water movement in a water conservation forest in hani terrace. *Water* 12 (12). <https://doi.org/10.3390/w12123520>.
- Sang, L.Y., Zhu, G.F., Qiu, D.D., Zhang, Z.X., Liu, Y.W., Zhao, K.L., Wang, L., Sun, Z.G., 2022. Spatial variability of runoff recharge sources and influence mechanisms in an arid mountain flow-producing zone. *Hydrol. Process.* 36 (8) <https://doi.org/10.1002/hyp.14642>.
- Sayama, T., McDonnell, J.J., 2009. A new time-space accounting scheme to predict stream water residence time and hydrograph source components at the watershed scale. *Water Resour. Res* 45 (7). <https://doi.org/10.1029/2008wr007549>.
- Shakoor, A., Shahbaz, M., Farooq, T.H., Sahar, N.E., Shahzad, S.M., Altaf, M.M., Ashraf, M., 2021. A global meta-analysis of greenhouse gases emission and crop yield under no-tillage as compared to conventional tillage. *Sci. Total Environ.* 750, 142299 <https://doi.org/10.1016/j.scitotenv.2020.142299>.
- Singh, N.K., Emanuel, R.E., McGlynn, B.L., Miniat, C.F., 2021. Soil moisture responses to rainfall: implications for runoff generation. *Water Resour. Res* 57 (9). <https://doi.org/10.1029/2020wr028827>.
- Skaalsveen, K., Ingram, J., Clarke, L.E., 2019. The effect of no-till farming on the soil functions of water purification and retention in north-western Europe: a literature review. *Soil Tillage Res* 189, 98–109. <https://doi.org/10.1016/j.still.2019.01.004>.
- Zhuo, L., Dai, Q., Han, D., 2020. Soil moisture sensor network design for hydrological applications. *Hydrol. Earth Syst. Sci.* 24 (5), 2577–2591. <https://doi.org/10.5194/hess-24-2577-2020>.
- Zoccarelli, D., Marra, F., Armon, M., Rinat, Y., Smith, A.J., Morin, E., 2019. Contrasting rainfall-runoff characteristics of floods in desert and Mediterranean basins. *Hydrol. Earth Syst. Sci.* 23 (6), 2665–2678. <https://doi.org/10.5194/hess-23-2665-2019>.
- Soil Survey Staff, 1999. Soil Taxonomy, A basic system of soil classification for making and interpreting soil surveys. second ed., Agric. Handb. No. 436, USDA Natural Resources Conserv. Serv., U.S. Govt. Print. Office, Washington, D.C., 160–162, 494–495.
- Song, X.F., Wang, S.Q., Xiao, G.Q., Wang, Z.M., Liu, X., Wang, P., 2009. A study of soil water movement combining soil water potential with stable isotopes at two sites of shallow groundwater areas in the North China Plain. *Hydrol. Process.* 23 (9), 1376–1388. <https://doi.org/10.1002/hyp.7267>.
- Sprenger, M., Leistert, H., Gimbel, K., Weiler, M., 2016a. Illuminating hydrological processes at the soil-vegetation-atmosphere interface with water stable isotopes. *Rev. Geophys.* 54 (3), 674–704. <https://doi.org/10.1002/2015rg000515>.
- Sprenger, M., Seeger, S., Blume, T., Weiler, M., 2016b. Travel times in the vadose zone: variability in space and time. *Water Resour. Res* 52 (8), 5727–5754. <https://doi.org/10.1002/2015wr018077>.
- Stock, B.C., Jackson, A.L., Ward, E.J., Parnell, A.C., Phillips, D.L., Semmens, B.X., 2018. Analyzing mixing systems using a new generation of Bayesian tracer mixing models. *PeerJ* 6, e5096. <https://doi.org/10.7717/peerj.5096>.
- Stumpff, C., Hendry, M.J., 2012. Spatial and temporal dynamics of water flow and solute transport in a heterogeneous glacial till: The application of high-resolution profiles of d18O and d2H in pore waters. *J. Hydrol.* 438–439, 203–214. <https://doi.org/10.1016/j.jhydrol.2012.03.024>.
- Sun, L., Yang, L., Chen, L.D., Li, S.J., Zhao, F.K., Sun, S.Q., 2019. Tracing the soil water response to autumn rainfall in different land uses at multi-day timescale in a subtropical zone. *Catena* 180, 355–364. <https://doi.org/10.1016/j.catena.2019.05.013>.
- Sun, Y., Zeng, Y., Shi, Q., Pan, X., Huang, S., 2015. No-tillage controls on runoff: a meta-analysis. *Soil Tillage Res* 153, 1–6. <https://doi.org/10.1016/j.still.2015.04.007>.
- Tao, T.T., Liu, L.S., Small, G.E., Chen, J.H., Wang, Y.Z., Sun, X., 2021. The effects of land management patterns on soil carbon sequestration and C:N:P stoichiometry in sloping croplands in southern China. *Agric., Ecosyst. Environ.* 320, 107584 <https://doi.org/10.1016/j.agee.2021.107584>.
- Thiros, N.E., Gardner, W.P., Kuhlman, K.L., 2021. Utilizing environmental tracers to reduce groundwater flow and transport model parameter uncertainties. *Water Resour. Res.* 57 (7) <https://doi.org/10.1029/2020wr028235>.
- Tipple, B.J., Jameel, Y., Chau, T.H., Mancuso, C.J., Bowen, G.J., Dufour, A., Chesson, L.A., Ehleringer, J.R., 2017. Stable hydrogen and oxygen isotopes of tap water reveal structure of the San Francisco Bay Area's water system and adjustments during a major drought. *Water Res* 119, 212–224. <https://doi.org/10.1016/j.watres.2017.04.022>.
- Tu, A., Xie, S., Zheng, H., Li, H., Li, Y., Mo, M., 2021. Long-term effects of living grass mulching on soil and water conservation and fruit yield of citrus orchard in south China. *Agr. Water Manag.* 252, 106897 <https://doi.org/10.1016/j.agwat.2021.106897>.
- Wang, H.X., Xu, J.L., Liu, X.J., Zhang, D., Li, L.W., Li, W., Sheng, L.X., 2019a. Effects of long-term application of organic fertilizer on improving organic matter content and retarding acidity in red soil from China. *Soil Tillage Res* 195, 104382. <https://doi.org/10.1016/j.still.2019.104382>.
- Wang, J., Fu, B.J., Lu, N., Zhang, L., 2017. Seasonal variation in water uptake patterns of three plant species based on stable isotopes in the semi-arid Loess Plateau. *Sci. Total Environ.* 609, 27–37. <https://doi.org/10.1016/j.scitotenv.2017.07.133>.
- Wang, J., Lu, N., Fu, B.J., 2019b. Inter-comparison of stable isotope mixing models for determining plant water source partitioning. *Sci. Total Environ.* 666, 685–693. <https://doi.org/10.1016/j.scitotenv.2019.02.262>.
- Wang, W., Sun, L., Wang, Y.H., Wang, Y.B., Yu, P.T., Xiong, W., Shafeeqe, M., Luo, Y., 2020. A convex distribution of vegetation along a stony soil slope due to subsurface flow in the semiarid Loess Plateau, northwest China. *J. Hydrol.* 586, 124861 <https://doi.org/10.1016/j.jhydrol.2020.124861>.
- Xiao, H.B., Xu, K., Zhan, Y.M., Wang, J., Wang, Z., Wang, L., Shi, Z.H., 2022. Physical structure and rainfall controls on subsurface hydrological connectivity in hillslope-riparian-stream continuums. *Catena* 214, 106286. <https://doi.org/10.1016/j.catena.2022.106286>.
- Xiao, L.G., Zhao, R.Q., Kuhn, N.J., 2019. Straw mulching is more important than no tillage in yield improvement on the Chinese Loess Plateau. *Soil Tillage Res.* 194, 104314 <https://doi.org/10.1016/j.still.2019.104314>.
- Xiao, X., Zhang, F., Che, T., Shi, X.N., Zeng, C., Wang, G.X., 2020. Changes in plot-scale runoff generation processes from the spring–summer transition period to the summer months in a permafrost-dominated catchment. *J. Hydrol.* 587, 124966 <https://doi.org/10.1016/j.jhydrol.2020.124966>.
- Xiao, X., Zhang, F., Li, X.Y., Zeng, C., Shi, X.N., Wu, H.W., Jagirani, M.D., Che, T., 2020b. Using stable isotopes to identify major flow pathways in a permafrost influenced alpine meadow hillslope during summer rainfall period. *Hydrol. Process.* 34 (5), 1104–1116. <https://doi.org/10.1002/hyp.13650>.
- Yang, S.H., Wu, H.Y., Song, X.D., Dong, Y., Zhao, X.R., Cao, Q., Yang, J.L., Zhang, G.L., 2020. Variation of deep nitrate in a typical red soil Critical Zone: Effects of land use and slope position. *Agric., Ecosyst. Environ.* 297, 106966 <https://doi.org/10.1016/j.agee.2020.106966>.
- Zhang, T., Li, J.H., Pu, J.B., Huo, W.J., Wang, S.N., 2021. Spatiotemporal variations of soil water stable isotopes in a small karst sinkhole basin. *Environ. Earth Sci.* 80 (1), 29. <https://doi.org/10.1007/s12665-020-09284-w>.
- Zhao, P., Tang, X.Y., Zhao, P., Wang, C., Tang, J.L., 2013. Tracing water flow from sloping farmland to streams using oxygen-18 isotope to study a small agricultural catchment in southwest China. *Soil Tillage Res* 134, 180–194. <https://doi.org/10.1016/j.still.2013.08.005>.
- Zhao, P., Tang, X.Y., Zhao, P., Zhang, W., Tang, J.L., 2016. Mixing of event and pre-event water in a shallow Entisol in sloping farmland based on isotopic and hydrometric measurements, SW China. *Hydrol. Process.* 30 (19), 3478–3493. <https://doi.org/10.1002/hyp.10867>.
- Zheng, W.B., Wang, S.Q., Sprenger, M., Liu, B.X., Cao, J.S., 2019. Response of soil water movement and groundwater recharge to extreme precipitation in a headwater catchment in the North China Plain. *J. Hydrol.* 576, 466–477. <https://doi.org/10.1016/j.jhydrol.2019.06.071>.
- Zhu, X., Chen, C.F., Wu, J., Yang, J.B., Zhang, W.J., Zou, X., Liu, W.J., Jiang, X.J., 2019. Can intercrops improve soil water infiltration and preferential flow in rubber-based agroforestry system? *Soil Tillage Res* 191, 327–339. <https://doi.org/10.1016/j.still.2019.04.017>.